

Machine learning-assisted multi-objective optimization of battery manufacturing from synthetic data generated by physics-based simulations



Marc Duquesnoy ^{a,b}, Chaoyue Liu ^{a,f}, Diana Zapata Dominguez ^{a,f}, Vishank Kumar ^d, Elixabete Ayerbe ^{b,c}, Alejandro A. Franco ^{a,b,e,f,*}

^a Laboratoire de Reactivité et Chimie des Solides (LRCS), UMR CNRS 7314, Université de Picardie Jules Verne, Hub de l'Energie, 15 rue Baudelocque, Amiens Cedex 80039, France

^b ALISTORE-European Research Institute, FR CNRS 3104, Hub de l'Energie, 15 rue Baudelocque, Amiens Cedex 80039, France

^c CIDETEC, Basque Research and Technology Alliance (BRTA), Po Miramón 196, Donostia-San Sebastian 20014, Spain

^d Umicore, New Business Incubation, 31 rue Marais, 1000 Brussels 8, Belgium

^e Institut Universitaire de France, 103 Boulevard Saint Michel, Paris 75005, France

^f Réseau sur le Stockage Electrochimique de l'Energie (RS2E), FR CNRS 3459, Hub de l'Energie, 15 rue Baudelocque, Amiens Cedex 80039, France

ABSTRACT

The optimization of the electrodes manufacturing process is critical to ensure high-quality Lithium-Ion Battery (LIB) cells, in particular for automotive applications. LIB electrode manufacturing is a complex process involving multiple steps and parameters. We have shown in our previous works that 3D-resolved physics-based models constitute very useful tools to provide insights into the impact of the manufacturing process parameters on the textural and performance properties of the electrodes. However, their high-throughput application for electrode properties optimization and inverse design of manufacturing parameters is limited due to the high computational cost associated with these models. In this work, we tackle this issue by proposing a generalizable and innovative approach, supported by a deterministic machine learning (ML)-assisted pipeline for multi-objective optimization of LIB electrode properties and inverse design of its manufacturing process. Firstly, the pipeline generates a synthetic dataset from physics-based simulations with low discrepancy sequences, that allows to sufficiently represent the manufacturing parameters space. Secondly, the generated dataset is used to train deterministic ML models to implement a fast multi-objective optimization, to identify an optimal electrode and the manufacturing parameters to adopt in order to fabricate it. Lastly, this electrode was successfully fabricated experimentally, proving that our modeling pipeline prediction is physical-relevant. Here, we demonstrate our pipeline for the simultaneous minimization of the electrode tortuosity factor and maximization of the effective electronic conductivity, the active surface area, and the density, all being parameters that affect the Li⁺ (de-)intercalation kinetics, ionic, and electronic transport properties of the electrode.

1. Introduction

Lithium-Ion Batteries (LIBs) represent the leading technology in the ongoing energy transition [1,2]. Such technology is deployed in many domains like portable devices and electric vehicles, due to their high performances and relatively good cell durability, while efforts heading to the emergence of gigafactories aim to decrease their massive production cost [3,4]. The latest signs of progress in the spectacular increase of cycle life, [5] higher energy and power densities, [6] are not only linked to the type of materials adopted but also to a meticulous optimization of the battery cell manufacturing process [7]. Nevertheless, such an optimization currently remains on trial-and-error, time-consuming, and costly approaches. It is believed that manufacturing scrap rates are between 5 and 30%, with the lowest values being more representative of production and the highest ones of prototyping

activities [8]. Indeed, the manufacturing process of LIBs is a complex procedure involving multiple interlinked steps and process parameters. Such steps are the electrode slurry preparation, the slurry coating and the drying, the calendering of the resulting electrode, the cell assembly, the electrolyte filling, and the formation [9]. Examples of the process parameters associated with these steps are the slurry formulation and solid content, the coating speed, the drying rate and the calendering pressure. Furthermore, trial-and-error optimization does not guarantee the achievement of the best electrode, because the multi-objective optimization (i.e., maximizing/minimizing multiple properties at the same time) is very challenging if it is only based on empirical approaches supported for instance on design of experiments [10]. Most of the time, the optimization of electrode properties lies on a specific target, limiting the effectiveness at the prototyping level due to multiple constraints [11, 12].

* Corresponding author.

E-mail address: alejandro.franco@u-picardie.fr (A.A. Franco).

The digitalization of the manufacturing process of LIBs is called to bring powerful tools to advance in understanding how manufacturing parameters impact electrode and cell properties (e.g., electrode porosity, tortuosity factor, conductivity, cell capacity), and to perform such optimization [13–16]. This digitalization is expected to be supported by physics-based modeling and machine learning (ML), simulating and analyzing each step of the manufacturing process and their interlinks, respectively. Our ERC-funded ARTISTIC project [17] pioneered this by bringing to the community a series of computational 3D-resolved physics-based models describing each step of the manufacturing process (from the slurry to the electrode performance) and being sequentially linked with each other, i.e., the output of a model is the input of the following model, and so on. For instance, Coarse-Grained Molecular Dynamics (CGMD) simulations are used to simulate, electrode slurries and their drying process in 3D synthetic uncalendared electrode mesostructures are generated as output (called mesostructures in the following) [13,18,19]. The Discrete Element Method (DEM) is used to simulate the calendering of such mesostructures [20]. The Lattice Boltzmann Method (LBM) simulates the electrolyte infiltration of the calendered electrodes taken alone or in the cell sandwich [16,21]. In addition, we directly use the results from these models in 4D electrochemical models simulating galvanostatic discharge-charge and electrochemical impedance spectroscopy, unlocking the relationships between manufacturing parameters, electrode mesostructure, and electrochemical performances [22,23,24,25]. These models were carefully validated in our experimental battery prototyping platform. They are being integrated into an online calculator, usable through any Internet browser, allowing to simulate the LIB manufacturing process without the need for computational skills. By November 2022, the updated version of this online calculator is being used by 515 researchers and students, with a significant percentage of users coming from industry [26].

While the ARTISTIC physics-based models are very useful for understanding and for analyzing the influence of manufacturing parameters on the 3D electrode mesostructures and their electrochemical performance, [20] they can have high computational costs (e.g., several hours are needed for simulating an electrode slurry), hindering their usage from performing fast (in few seconds) electrode optimizations. Such fast optimization capabilities will be needed in digital twins collecting data through sensors and giving instructions to the manufacturing machines with actuators for on-the-fly and autonomous optimization [27–29,15]. In the ARTISTIC project, we have demonstrated that ML can also constitute a powerful tool for unraveling correlations between manufacturing process parameters and electrode properties [30,31,32]. ML has also demonstrated powerful capabilities to solve a wide diversity of scientific problems in the battery field [33–35]. For instance, Tong et al. applied Neural Networks to predict LIB's Remaining Useful Life [36]. Turetskyy et al. used regression models to build a multi-output model predicting the final product properties of a battery production line [37]. Furthermore, ML has been used to derive predictive models from physics-based models describing LIB aging or redox flow battery operation [38,39]. These models reproduce the prediction capabilities of the physics-based models with much cheaper computational costs. Furthermore, algorithms like the Bayesian Optimization (BO) framework supported by a probabilistic approach, constitutes powerful tools to solve optimization problems and perform inverse design [40,41,42,43]. BO has seen widespread applications in different domains such as cognitive science, [44] autonomous driving, [45] and pharmaceutical product development [46]. More recently, Wang et al. reviewed the interest of BO in chemical product discovery and materials modeling [47]. With a multi-objective approach, Jiang et al. quantified the decrease of a LIB charging time for single and multi-constant-current-step charging profiles, [48] while Gaonkar et al. optimized cell designs (thickness and porosity of LIB electrodes) for various scenarios that have high energy density and low-capacity fade by using data calculated with a Newman model [49].

In view of the BO blooming [50], it is natural to think that multi-objective BO is an interesting approach to explore in the context of battery electrode manufacturing.

In this work, we report an innovative computational approach able to optimize multiple essential electrode properties simultaneously and able to evaluate the process parameters to adopt in order to manufacture them. We first generated a synthetic dataset containing inputs/outputs from a stack of ARTISTIC physics-based models simulating a $\text{LiNi}_{1/3}\text{Mn}_{1/3}\text{Co}_{1/3}\text{O}_2$ (NMC-111) active material-based electrode manufacturing process, using low discrepancy quasi-random sequences [51]. This enabled us to define a batch of sparse manufacturing conditions and evaluate the properties of the various digitally generated electrode mesostructures. The result constitutes a meaningful dataset for the training/testing of deterministic learning models, whose main goal is to approximate each expensive electrode physics-based generation as a numerical function of the manufacturing parameters. These so-derived models cover the overall available manufacturing parameters space when proceeding with the training, and bypass the manufacturing physical modeling chain as illustrated in Fig. 1. Secondly, we took advantage of combining these models to raise a deterministic-assisted objective function for maximizing/minimizing selected properties simultaneously, without the need to launch the physics-based models. This is carried out by embedding the latter functions into a BO framework for this multi-objective optimization purpose. Our synthetic dataset accounts for the slurry, drying, and the resulting calendered electrode, for the determination of the best amount of active material (AM%), slurry solid content (SC%), and the calendering compression degree (CD%, referring here to the percentage of electrode thickness reduction versus the initial thickness), giving an electrode with minimal tortuosity factor, maximal effective electronic conductivity, maximal active surface area between AM and pores, and maximal density. Such optimized properties are expected to influence the kinetic, ionic, and electronic transport properties of the electrodes. The so-found best manufacturing condition was finally used to manufacture a real electrode to propose a practical application at the experimental level, showing that it is possible to design electrodes using the best manufacturing parameters resulting from the multi-objective optimization. In the following, we explain our approach in detail, present the results, and explain why we believe this work paves the way toward the emergence of autonomous battery manufacturing optimization procedures.

2. Low discrepancy sequences for a design of experiments

Given the high computational cost of the physics-based manufacturing process modeling that consumes resources and time to generate highly-representative data, it is essential to find a computationally cheaper and more automatic way to probe such a space (called hereafter the input space). To do so, we generate a design of experiments (DOE) based on highly-representative manufacturing parameter values, which were used as inputs of the physics-based models for the data generation (electrode mesostructures and associated properties) [52]. This was done by applying quasi-random Sobol sequences with Saltelli extension (Fig. 2) [53]. Such sequences sample quasi-uniform distributions of data from continuous input parameters, and properly probe the input space to capture all of his sub-areas accurately. These sequences propose a low discrepancy of data points contrary to more common distributions, such as Gaussian or uniform distributions, which is particularly true when the number of points is limited. Figure S1 in the Supplementary Information compares the low-discrepancy sequences versus Gaussian and uniform distributions for a different amount of data points, illustrating our choice of Sobol sequences to generate the DOE [51]. In our case study, we used as input parameters the AM% and the SC % related to the slurry step, and the CD% related to the calendering step, and then selected fixed boundaries for each of them, to form the input space illustrated by the hyper-rectangle in Fig. 2.

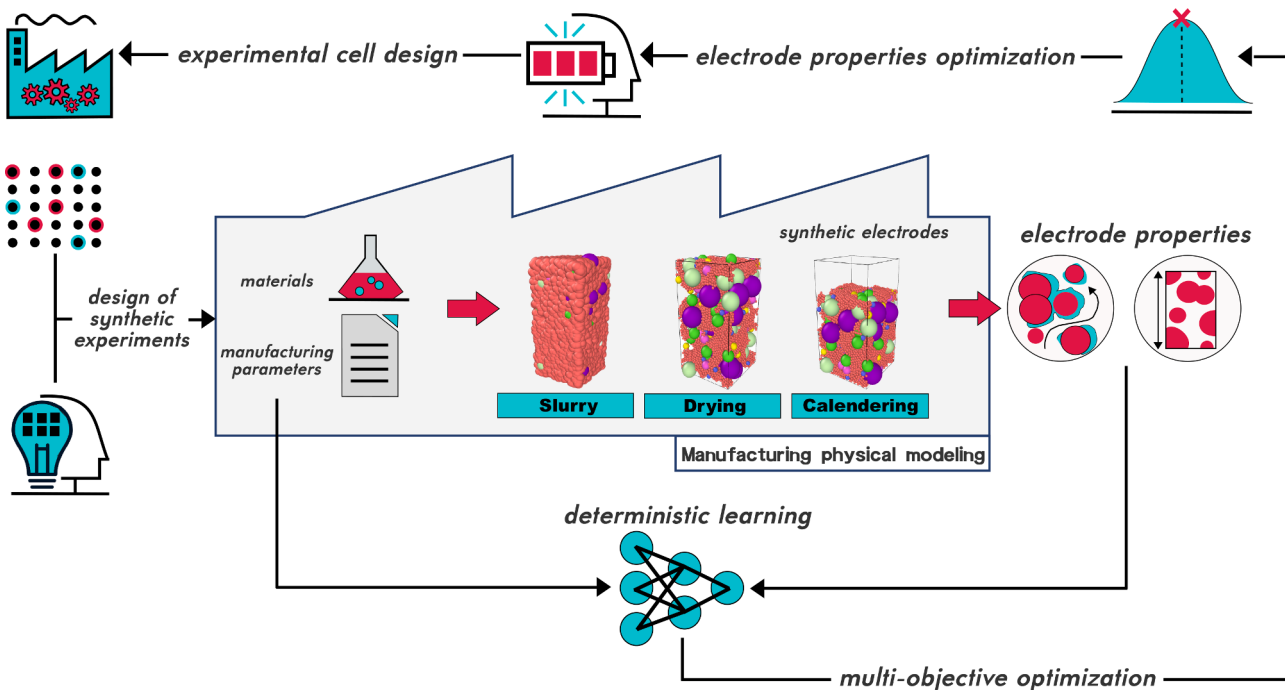


Fig. 1. Schematic representation of our deterministic-assisted multi-objective optimization of electrode properties to design better lithium-ion batteries. The manufacturing process modeling from the slurry to the calendering is carried out through a chain of interlinked 3D physics-based models for the prediction of electrode mesostructures whose textural properties are evaluated. The coupling of a low discrepancy manufacturing parameters sequences with a deterministic learning allows bypassing the entire manufacturing physics-based modeling in the first step, then serving for the implementation of the optimization loop in the second step. The approach allows pinpointing the manufacturing parameters that have to be used in order to fabricate an electrode with optimal properties.

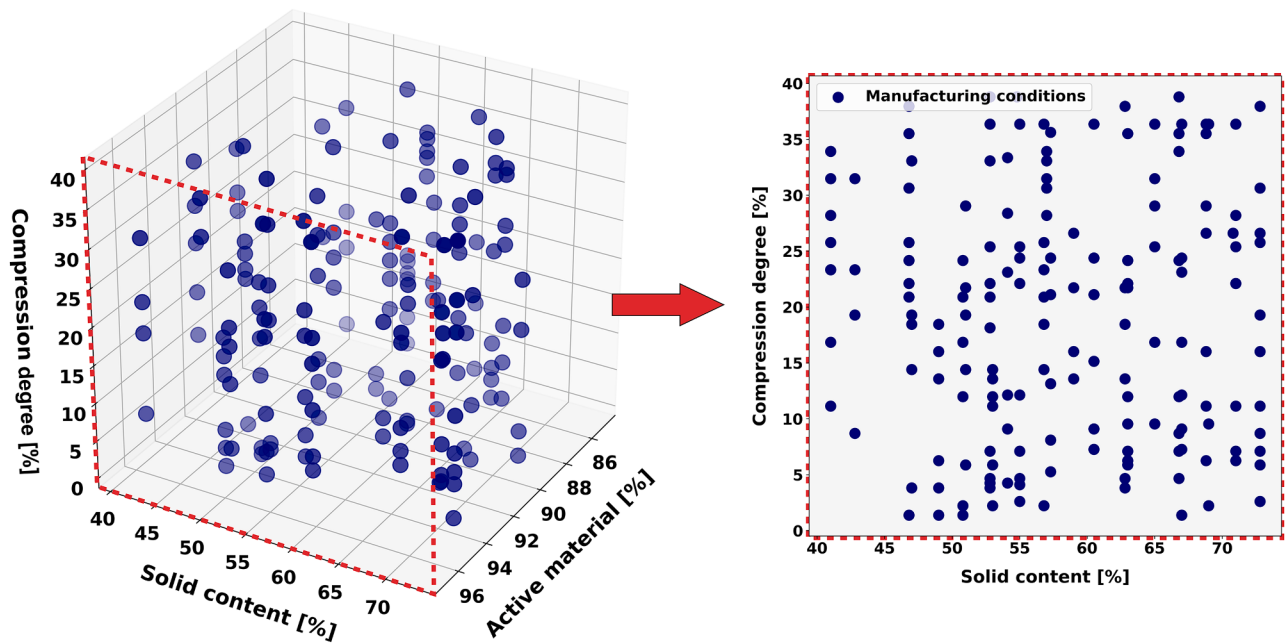


Fig. 2. Design of experiments for the synthetic dataset through the Sobol sequences after the sampling modifications within our input space. The 3D representation is straightforward due to a space-filling hyper-rectangle design. A 2D representation of the generated sequences based on the CD% values as a function of SC% values displays the quasi-randomness of the input space-filling.

In our manufacturing physics-based modeling workflow, the generation of a slurry and its corresponding dried electrode is computationally expensive (e.g., ~150 hours), while the generation of a calendered electrode is drastically faster (e.g., ~8 hours). As a consequence, we proceeded to a post-treatment of the quasi-random sequences regarding the variables AM%, and SC% (inputs of the slurry physics-based

modeling) to tackle the overall high computational cost. This post-treatment consisted in selecting a limited amount of slurry manufacturing parameter values (AM%; SC%) among those generated in the DOE and associating them randomly to the evaluations of CD% values generated by the quasi-random sequences. In the end, our DOE corresponded to a shortened quasi-random generation of diverse slurries

(and associated drying) where different quasi-random calendering conditions can be associated with one specific electrode slurry. In particular, this DOE was shortened to reduce the computational time when generating the associated 3D mesostructures, whereas its representativity from the input space was meaningful, as displayed in Fig. 2. According to Cervellera et al., this strategy of sequence generation widely influences the results in ML applications and optimization processes [54].

3. Data acquisition

For each set of manufacturing parameter values (AM%, SC%, CD%) in the DOE, we generated the different 3D NMC111 electrode mesostructures by using the ARTISTIC physics-based models simulating the slurry, the drying, and the calendering of the resulting electrodes [19,23, 55]. These models were developed under the LAMMPS software and have been already calibrated and validated with experimental data from the battery production pilot line available in our laboratory [56]. They were launched on the computational cluster MatriCs (located at the Université de Picardie Jules Verne (UPJV)), using eight nodes (384GB of RAM each), each composed of two processors (Intel Xeon Gold 6148 CPU @ 2.40 GHz, 20 cores) [57]. We initialized the total mass of an electrode slurry to 0.1 µg since we considered a small electrode volume (with a bottom surface area around 400–900 µm²) to decrease the computational cost and to ensure the resulting mass loadings will match the ones found from our experiments (about 15–40 mg/cm²). We processed the mesoscale simulated Nickel-Manganese-Cobalt (NMC111)-based slurry through a top-down approach, supported by the Coarse-Grained Molecular Dynamics (CGMD) [13]. This model accounts for spherical representations of particles which is sufficient for NMC111 electrodes, as we have already demonstrated in our previous publications. The simulation encompasses Force-Field parameters (FFs) to describe the physicochemical interaction between active material (AM) and carbon-binder domain (CBD) phases during the slurry equilibration [13]. Then, the dried electrode mesostructure was obtained by uniformly shrinking the CBD particles to mimic the solvent removal and get the equilibrated electrode mesostructure [19]. With the obtained dried mesostructure, we proceeded to the calendering of the resulting dried electrode by using the DEM which simulates the mechanical behavior of the electrode upon compression [20,55]. The resulting calendered electrode mesostructures were characterized in terms of thickness, volumes, densities, and active surface areas (surface of contact between AM particles and the pores within the electrode, by assuming that the pores can be fully filled with the electrolyte) using in-house Python scripts, their effective electronic conductivities using GeoDict, [58] and their tortuosity factors of the pore network using TauFactor (see the Supplementary Information for the details about the calculations of the tortuosity factor) [59]. Fig. 3 illustrates the communication between the different software for handling the mesostructures when extracting the electrode properties. In total, it took two months to

generate the synthetic dataset, including 174 different manufacturing conditions generating the corresponding mesostructures for the slurry, drying, and calendering steps.

3.1. Deterministic learning

The calculated 3D electrode properties versus manufacturing parameter values constitute a meaningful database for training a deterministic learning (i.e., regression functions trained on a pre-defined dataset). Indeed, we replaced the entire manufacturing physics-based modeling chain (illustrated in Fig. 3) with regression models to directly calculate the electrode properties as a function of the manufacturing parameters. Since the synthetic dataset covers the input space well, the latter learning can calculate the electrode properties regardless of the manufacturing conditions accurately [60]. This was concluded thanks to the training and testing of the Sure Independence Screening and Sparsifying Operator (SISSE) algorithm, according to good capabilities to interpolate within the input space. SISSE allows directly obtaining a mathematical equation interlinking electrode properties with manufacturing parameters, which is something convenient for proceeding into the optimization process [61–63]. The algorithm mentioned above mainly provides a linear relationship between an output y (electrode property) and a set of descriptors $(d_i)_{i < n}$ formed by non-linear relationships between inputs (manufacturing parameters), defined as

$$y = \sum_{i=0}^n c_i \times d_i, c_i \neq 0 \quad (1)$$

The equation above lies on two pillars: one based on the feature space construction for descriptors implementation, [64] and the second one on a solution algorithm for the error minimization [65,66]. We have included detailed explanations about the algorithm in the Supplementary Information. The validation of the deterministic learning was achieved by analyzing relevant validation metrics discussed in the following section.

3.2. Optimization process

Once the training of the deterministic learning is done, we proceeded to a Bayesian multi-objective optimization to assess an objective function (denoted (C_f)), itself dependent on the deterministic learning. We built a scalarizing function after transforming the multi-objective problem into a single objective function. In that sense, one popular way to apply BO for multi-objective optimization problems is using Gaussian Process (GP) regressions as the model to approximate (C_f) . In each iteration, BO calculates a posterior distribution $(C_f) | D$ over (C_f) regarding the set of all previous data D . Then, this proposes a new set of manufacturing parameter values, chosen by an acquisition function, balancing between the exploitation of prior parameter value combinations to identify nearby minima, and the exploration to identify minima

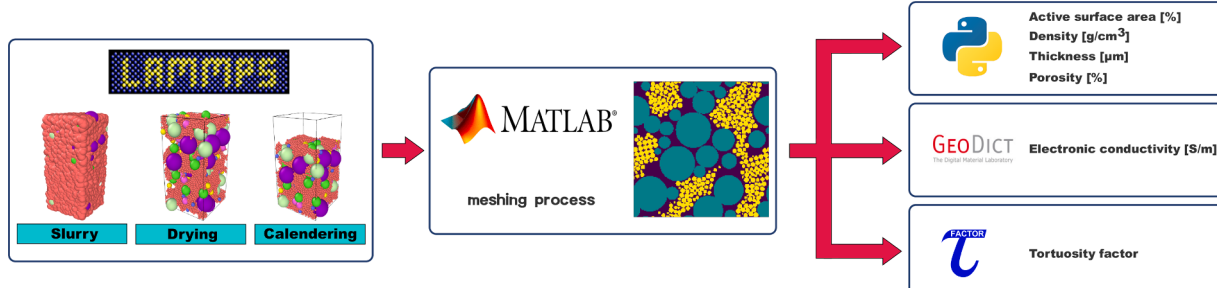


Fig. 3. Schematic representation of the link between the different software for the handling of the 3D electrode mesostructures for the data acquisition generated by the physics-based modeling workflow. This starts with the simulations from the slurry to the calendering, where the resulting electrode is meshed in order to serve as input of the different codes for the properties calculation.

far from prior parameter value combinations [67,68]. The GP model is updated at each step until the BO returns the manufacturing parameter values giving origin to an electrode with the optimal properties [69,40]. In this study, we assessed a minimization problem to figure out the optimization of the electrode electrochemical performance and electronic/ionic transport efficiency by formalizing the search for the best manufacturing parameter values x giving the best electrode as it follows:

$$x^* = \operatorname{argmin}_x (C_f(x)) \quad (2)$$

We maximized the effective electronic conductivity, the density, and the active surface area between AM and pores simultaneously, the latter being assumed to be fully filled with the electrolyte, and we minimized the tortuosity factor. This multi-objective optimization was done by granting equal weights (i.e., 1/4) to each property without constraints on the manufacturing parameters due to their independence between each other. We considered this equal balance for our proof of concept. According to different orders of magnitudes, we adopted a scalarization method for (C_f) through the incorporation of a scalar fitness function, allowing to fit each property value into [0, 1] when calculating the objective function values. This scalarization avoids a bias induced by the property values, balancing the objective function between the maximization of some of the properties and the minimization of the others [41]. Each scaled electrode property (denoted $(y_{i,x}) \forall i \leq 4$) was included in (C_f) in order to minimize $(y_{i,x})$ when the associated property used to be minimized, and to minimize $(1 - y_{i,x})$ when the property used to be maximized. In this regard, we proposed a (C_f) satisfying the points above by an equal-weighted power function as it follows [67]

$$C_f = \frac{1}{4} \times \left(\sum_{y_{i,x} \in Y_m} (y_{i,x})^2 + \sum_{y_{i,x} \in Y_M} (1 - y_{i,x})^2 \right) \quad (3)$$

where Y_m and Y_M denote respectively the set of electrode properties that are minimized and maximized in our study.

In addition, (C_f) was built with mathematical equations from the deterministic learning, predicting the property as a function of a specific set of manufacturing parameter values x . Consequently, the objective function calculations were a quick non-linear combination of predictions without running the entire manufacturing process physics-based modeling chain. This presents the advantage of a reduced computational cost in assessing the multi-objective optimization process and obtaining the best manufacturing parameter values associated with the optimal electrode.

4. Results

4.1. Validation of the deterministic learning

The root mean square error in percentage (RMSE%) and the R^2_{score} for the goodness of fit, were chosen as validation metrics to evaluate and validate the training/testing of the deterministic learning. As a standard practice in ML, the whole dataset has been divided randomly into training and testing datasets for model training and validation, respectively [70]. The training dataset contained 80% of data, randomly picked up from the synthetic dataset which contains 174 sets of manufacturing parameter values in total, and the testing dataset contains the remaining 20%. In Table 1, we report the values for the testing dataset, where the results are supported by the regression plots displayed in Figure S1 in the Supplementary Information. We also reported the values for the training dataset in Table S1 in the Supplementary Information. Even though we obtained very high R^2_{score} values and low RMSE% values, we repeated the training/testing process by randomly changing the split 75 times, and determined the 95% confidence interval (CI95) for the R^2_{score} [71]. The latter interval provides more statistical analytics on the capabilities of the SISSO algorithm to train/test regardless of the seed of the re-sampling procedure for our shortened

Table 1

Validation metrics are calculated over the testing dataset and associated with the fitting of the electrode properties. The 95% confidence interval (CI95) were estimated with a total of 75 random seeds of training/testing datasets for the uncertainty of the R^2_{score} .

Property	RMSE%	R^2_{score}	CI95
Tortuosity	1.48	0.933	[0.941; 0.950]
Conductivity [S/m]	7.80	0.979	[0.978; 0.981]
Active surface AM/Electrolyte [%]	1.41	0.911	[0.885; 0.914]
Density [g/cm ³]	1.87	0.968	[0.962; 0.971]

dataset. Indeed, confidence intervals estimate the variability of the metrics on how precise it is likely to be. Therefore, there is a 95% likelihood that our CI95 covers the ranges detailed in Table 1, reporting the true learning performance [72].

At the end, the results showed high predictive capabilities of the deterministic learning to predict the electrode properties only by giving the three manufacturing parameters as inputs. The CI95s did not have extended boundaries for the selected 95% likelihood, with values very close to 1 being the limit value of such a metric. Also, the different RMSE % are mainly very low and confirm good predictive capabilities. All of these points suggest that the resulting deterministic learning is accurate enough regardless of the seed with the training/testing, without any bias from the synthetic dataset. This suggests that the trained deterministic learning was a suitable regression model to predict the kinetic, ionic, and electronic transport properties, thus bypassing the entire manufacturing physics-based modeling chain.

4.2. Optimal manufacturing parameter values

The BO framework was designed with 300 iterations as a cut-off to propose a meaningful candidate for the minimization of the objective function. Fig. 4 shows the 2D partial dependence plot (PDP), allowing us to interpret the importance of the different manufacturing parameters in the GP model. The principle lies in the visualization of the marginal effect of manufacturing parameters on the approximation of (C_f) values, given an average influence of all the other parameters. Since the input parameters are uncorrelated, the 2D partial dependence plot is a tool to interpret how predictions of the objective function change when fixing one manufacturing parameter value every time and by freeing the other two [73]. Following the results from Fig. 4, the in/sensitivity regions of the input space are not affected by the application of the deterministic learning due to its low prediction error and low variability during the training processes. The latter provides a high-performant objective function to replace the common physics-based models for electrode properties calculations.

As a result, it can be seen that the optimal solution (yellow star) is located nearby the region of SC% and CD% with low partial dependence giving no high variability of the objective function in that region of the space. In contrast to this result, the influence of AM% values is less obvious and more independent at higher values of AM% (> 92%), suggesting more variability of that parameters to find the optimal value with a less straightforward marginal effect of AM%. Nevertheless, Fig. 4 displays that the aggregation of manufacturing parameter values as candidates tested by the BO framework, falls into the region of the input space where the optimal solution is located. This highlights the rapidity of the BO in finding the region of the best candidate, as it can also be seen through the convergence plot from Figure S3 in the Supplementary Information.

In such a way, we were able to obtain the best values of the three manufacturing parameters that optimize the electrode properties of interest simultaneously and that do not represent the extreme values of the manufacturing parameters ranges used in the BO framework. This set of manufacturing parameters was reported in Table 2.

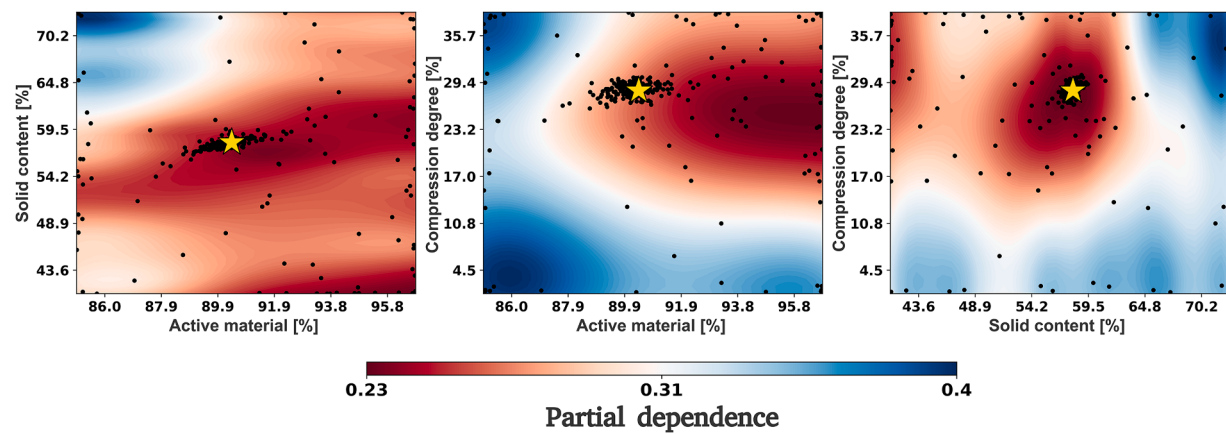


Fig. 4. Partial dependence plots allowing to interpret the GP model's predictions. A 2D representation was straightforward to better visualize how manufacturing parameter values influence (C_f) values for the search of the optimal manufacturing condition. The results are color-coded where warmer values suggest less variability in the predictions when changing the hidden input parameter values, contrary to cooler values which suggest higher variability. The yellow stars point out the pairwise optimal manufacturing conditions predicted by the BO framework. The black dots represent each new possible candidates of manufacturing parameters to be explored as the solution in the optimization loop, with most of them that are concentrate around the global minimum.

Table 2
Optimal manufacturing parameters predicted by the BO framework.

Active material [%]	Solid content [%]	Compression degree [%]
90.4	58.1	28.4

5. Discussions

5.1. Optimized transport properties

The four output properties (electronic conductivity, active surface area, tortuosity factor, and density) correspond to different electrochemical characteristics during the LIB electrode operation. For instance, the electronic conductivity affects the solid phase electrostatic potential gradient. The active surface area affects the reaction kinetics and the associated current density on the surface of the AM. Under a certain terminal current, a higher active surface area means a lower reaction current density. According to the Butler-Volmer equation, the overpotential of the reaction is reduced [74]. The tortuosity factor is related to the effective diffusivity of Li^+ in the electrolyte and ionic conductivity. The lower the tortuosity factor is, the easier it is for ions to transport. The density is vital for the evaluation of the volumetric energy density of the electrode. To achieve the highest energy density, the electrode should have the highest active surface area, the highest electronic conductivity, and the highest density, with a tortuosity factor equal to 1. However, in practice, these four properties are related to each other. Therefore, an optimized electrode will result from a balance between the values of these properties, with the best performance achievable under the constraint of the manufacturing parameter space.

Fig. 5B displays the pack of generated 3D electrode mesostructures using the optimal manufacturing parameters from Table 2 as inputs of the physics-based modeling chain. The associated four electrode properties were extracted from these mesostructures and were displayed in the radar chart from Fig. 5A. Furthermore, we reported the comparison of these values with the ones predicted by the deterministic learning in Table 3. As can be noticed first, there is a good match between the values extracted from the mesostructures and the predictions, supporting the physical relevance of our deterministic approach to predict the electrode properties within the optimization workflow correctly. Secondly, the same radar chart reflects a good balance for maximization/minimization of the four properties, affording a high conductivity, and low tortuosity as an example. Besides, the Kernel Density Estimation (KDE) for each property reflects the localization of the optimal electrode properties

values compared to the empirical distribution of values from the synthetic dataset. This representation emphasizes the multi-objective optimization predictions for a high-performance mesostructure without any extreme case in terms of one electrode property, especially because it is not possible to obtain the lowest tortuosity factor and the high conductivity at the same time due to the limitations of the physics-based models. For instance, the KDE displays a high optimal conductivity (0.175 S/m), while the highest values are less illustrated within our synthetic dataset. The optimal density seems here to be close to the mean value from the KDE, concluding on the difficulty of obtaining a higher value for optimizing the other properties at the same time.

In Fig. 6, we compare the optimal case with four extreme cases of electrodes from the synthetic dataset, each of them having the highest performance for only one property. We report the corresponding manufacturing conditions in Table S2 in the Supplementary Information. In the first case (blue vs. red), the electronic conductivity is pushed to the extreme by increasing the content of the CBD phase and then reducing AM%. This leads to a low electrostatic potential gradient in the solid (AM+CBD). In the meantime, more AM surface area is covered by the CBD phase. According to previous research, the CBD phase is a porous conductive matrix, with a porosity of approximately 50% for some electrode formulations [75]. The low degree of exposure of AM to the pores will increase the surface reaction current density, triggering a higher Li^+ (de-)intercalation reaction overpotential. Furthermore, the effective electronic conductivity and diffusivity within the CBD phase were 5% of the bulk phase [76]. Therefore, this results in a lower effective diffusivity in the whole electrode. The optimal case, on the contrary, has a higher active surface area and density, which is in favor of obtaining a higher energy density.

Case 2 (green vs. red) illustrates the comparison with the tortuosity factor-optimized electrode. The low tortuosity factor results from the low compression degree of this electrode (2.24%). From a manufacturing process viewpoint, this case is close to an uncalendared electrode. It is worth to be noticed that the electronic conductivity drops due to the poor connection between the CBD particles. Electrode capacity can be severely undermined without a well-established electronic conductive network. While increasing electrostatic potential drop in the solid phase can also cause particles isolation and inactivation. Case 3 (yellow vs. red) aimed at the high active surface area. From the manufacturing process perspective, this is the case where solid content is rather high (60.3%), which is a favorable way to increase the electrode energy density. The cost of raising density while maintaining a porosity of 40% is reduced CBD content. The conductivity is more than two times lower than the optimal case. Case 4 (magenta vs. red) exhibits the

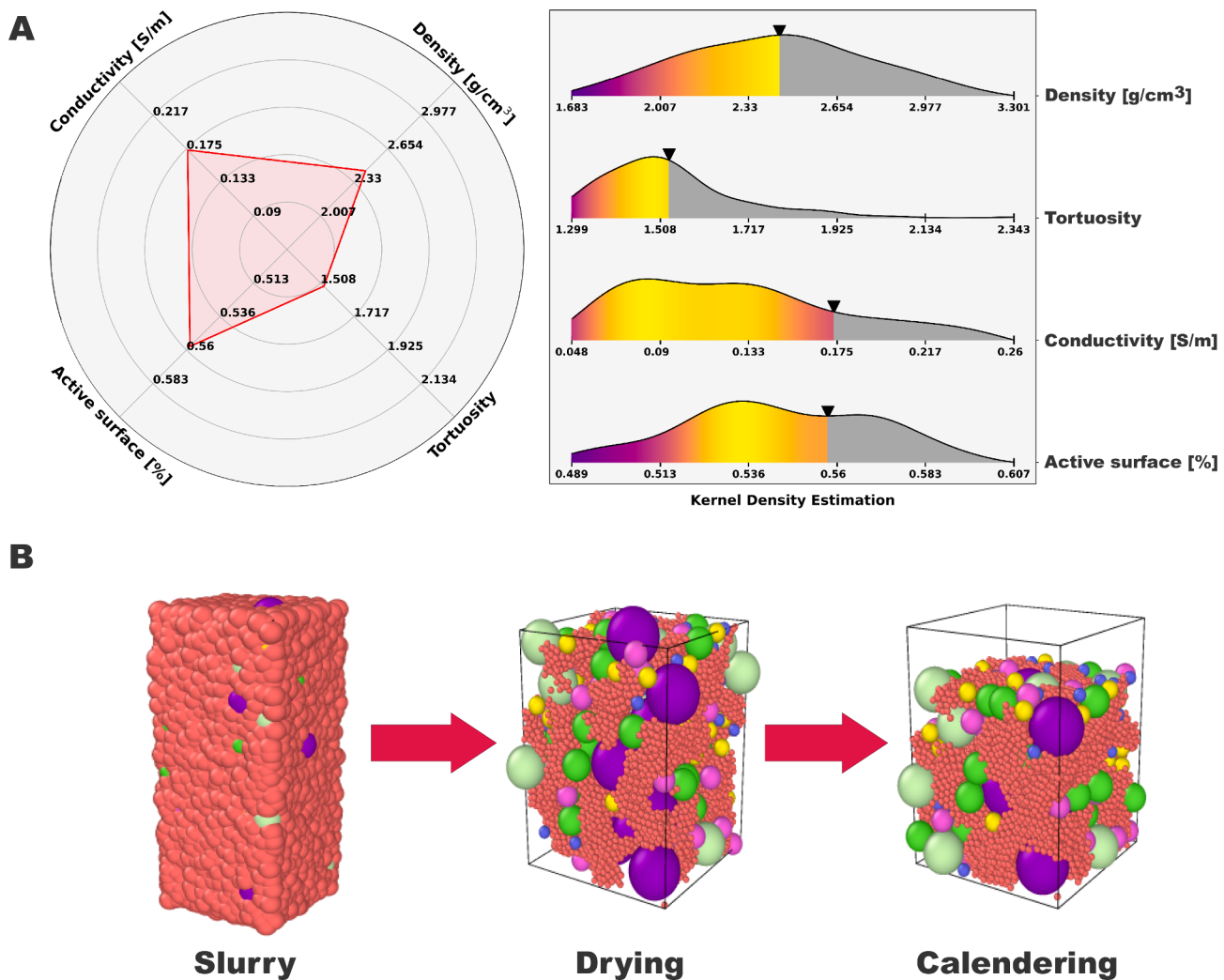


Fig. 5. (A) Graphical representation of the optimized electrode properties obtained through the deterministic-assisted optimization loop. A radar chart displays the optimized values after generating the 3D electrode mesostructures using the optimal manufacturing condition. The values have been scaled between the min and max for each property from the synthetic dataset. A Kernel Density Estimation was added in order to display how the optimized values are represented within the empirical distribution of properties from the synthetic dataset. A gradient color-codes such a distribution until the optimized value. We replaced electronic conductivity with conductivity, tortuosity factor with tortuosity, and active surface area with active surface in this Figure. (B) 3D electrode mesostructures from the slurry to the calendering step associated with the optimal manufacturing condition predicted by the deterministic-assisted optimization loop.

Table 3

Comparison of electrode properties using the deterministic learning and the generated 3D electrode mesostructures (physics-based models). Both used the optimal manufacturing condition as input parameters.

Property	Deterministic learning	Physics-based model
Tortuosity	1.4700	1.5286
Conductivity [S/m]	0.1724	0.1750
Active surface AM/Electrolyte [%]	54.0522	55.7230
Density [g/cm^3]	2.4459	2.4456

highest density due to a large compression degree (36.36%). The highly compact structure dramatically increases the tortuosity factor and decreases the active surface area. In reality, there is a risk of breaking AM particles alongside the increased overpotential, which is not considered in the current version of our optimization workflow. The newly generated surface of the crack in the AM particles can cause extra parasitic reactions, such as Cathode Electrolyte Interface CEI growth and transition metal dissolution. The pulverized particles can also lose connection with the conductive network, becoming inactive. Our multi-objective

optimization pipeline allows us to suggest an optimal electrode for moderate calendering conditions typically used in battery prototyping lines.

It is worth noticing that our optimal electrode result is acquired based on the weight we put on each property according to Eq. 3. In our work, these weights have been selected to equally balance the textural properties of calendered electrodes. Depending on different electrode systems, manufacturing steps considered (e.g. solid electrolyte interphase formation), or manufacturing conditions, the weights can be further adjusted. This results in different optimal cases regarding the final battery cell application from an industrial perspective (e.g., fast-charging and high-power applications, cell durability). Indeed, the real battery cell performance depends on how we adjust the electrode properties to assess the best electrode properties. Maximizing the energy density would result in giving more weight on the density compared to the other electrode properties, whereas maximizing the power density implying focusing more on the tortuosity and conductivity. In that sense, our optimization workflow can be generalized to any kind of optimization problem for different applications.

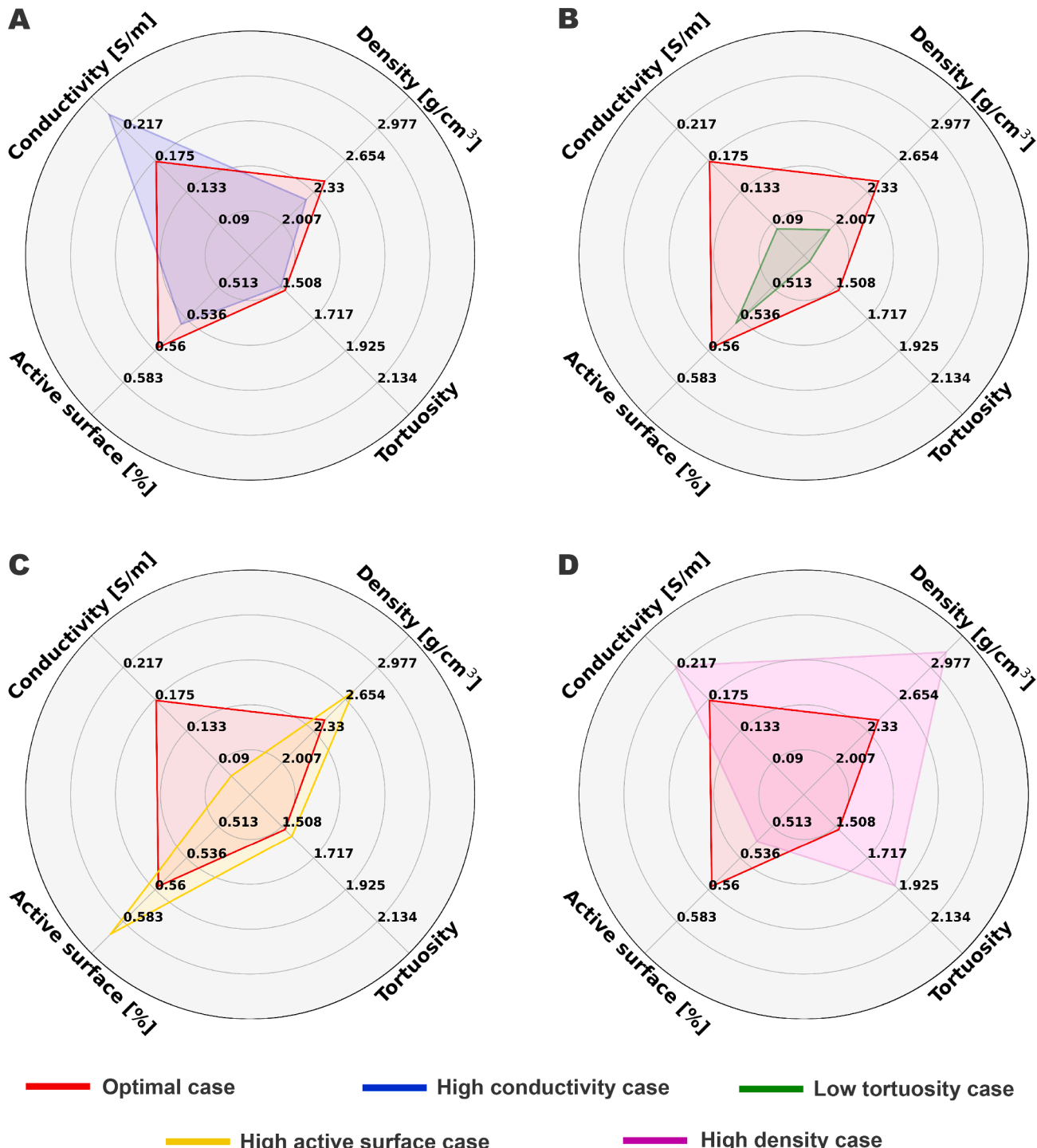


Fig. 6. Radar chart plots comparing the optimized electrode properties with extreme cases from the synthetic dataset. Each plot shows the interest to obtain the optimal case (red) instead of having a high-performance electrode for only one property. We replaced electronic conductivity by conductivity, tortuosity factor by tortuosity, and active surface area by active surface in this Figure. (A) High electronic conductivity case ((AM%, SC%, CD%) = (86.3%, 57%, 33.08%)) with a porosity of 26.55%; (B) Low tortuosity factor case ((AM%, SC%, CD%) = (88.8%, 56.8%, 2.24%)) with a porosity of 42.35%; (C) High active surface area case ((AM %, SC%, CD%) = (96.5%, 60.3%, 9.11%)) with a porosity of 35.97%; (D) High density case ((AM%, SC%, CD%) = (94.5%, 71%, 36.36%)) with a porosity of 24.11%.

5.2. Experimental relevance of the predicted optimal electrode

In order to assess the experimental relevance of the optimal electrode predicted by our multi-objective optimization pipeline (Fig. 5), we used the corresponding manufacturing parameter values to manufacture such an electrode by using our battery prototyping line. To avoid calibration errors in the prototyping machines, we have rounded the manufacturing

parameter values suggested by our BO framework. Even though our 3D physics-based models did not take into account all the manufacturing parameters that can be tuned in the prototyping machines (e.g., slurry drying temperature), we have adjusted the coating comma gap and the coating speed, and the temperatures of the two-part oven of our prototyping line in order to fix meaningful values to match the optimized electrode properties proposed by our BO framework (see the Methods

section). The resulting experimental properties are reported in **Table 4** showing a reasonable agreement when compared to the modeling results reported in **Fig. 5**. We have constrained our comparison between the experimental and optimized electrode properties obtained by our BO framework to porosity, density, thickness, mass loading, and tortuosity since the conductivity was not experimentally evaluated (see Experimental section). The main difference between the physical-based modeling workflow (for generating the electrodes on which this optimization work was based) and the experimental process is that the physics-based modeling workflow mentioned above uses as departing components sphere particles that allow us to reduce computational cost. In addition, our physics-based models use the clustered entity CBD, which is also considered for simplifying the calculations, and it is different from experimental electrode slurry formulations since the carbon black and binder compositions are considered on their own. This is why some discrepancies may be found between the model-predicted results and the measured values.

Despite these approximations in the physics-based modeling workflow, it is worth mentioning that it has demonstrated a satisfactory match with experimental results such as electrode slurry viscosity and density, dried and calendered electrode porosity, etc. [13,20,24]. With the purpose to support the interest of the so-calculated experimental properties from **Table 4**, we have included in the Supplementary Information a comparison between these properties and others from extreme experimental conditions. This spotlights the physical relevance of the electrode properties that have been determined using the predicted best manufacturing conditions, and show that we obtained relatively interesting properties for the experimental electrode.

The synthetic dataset can be extended to other binder systems by optimizing the values of the Force Field parameters in our CGMD and DEM approaches. This can be done by calculating experimental observables using the virtually generated slurries and electrodes and comparing them with the experimental counterparts. Such observables include the electrode slurry viscosity as a function of the applied shear rate, the slurry density, and the electrode porosity upon drying and calendering as a function of the drying rate and the electrode compression degree, respectively. The optimization can be done using optimization algorithms, as we have demonstrated already in our previous publications [78]. Under this scenario, a new set of electrode systems can be generated using the physics-based modeling workflow to perform our multi-objective optimization of the manufacturing with another type of binder. Regarding other electrode systems, such as the ones containing graphite with heterogeneous particles, we recently improved our physics-based modeling workflow for the use of non-spherical active material particles that will be implemented by us in future manufacturing optimization studies [79]. This highlights the relevance of our approach to give a practical application, an innovative proof of concept from the manufacturing physics-based modeling optimization, reducing experimental time and cost and suggesting new designs of high-performance cells.

Table 4

Properties of the cathode electrode experimentally manufactured with the manufacturing parameter values evaluated as optimal by the optimization pipeline. Tortuosity factors were calculated by using the Transmission Line method proposed by Landesfeind et al. (details provided in the Supplementary Information) [77].

Property	Pristine	Calendered 30%
Mass loading [mg/cm ²]	6.7 +/- 0.3	6.7 +/- 0.3
Thickness [μm]	68 +/- 4	48 +/- 4
Density [g/cm ³]	1.6 +/- 0.4	2.6 +/- 0.3
Tortuosity factor	3.5 +/- 0.5	1.8 +/- 0.4
Porosity [%]	60 +/- 0.3	29 +/- 0.7

Conclusions

In this study, we reported an innovative deterministic-assisted multi-objective optimization approach of different LIB electrode properties (related to kinetics, electronic and ionic transport) simultaneously. Such an approach predicts the process parameters to adopt in order to manufacture the so-found optimal electrode. To do so, we took advantage of the previously developed 3D-resolved ARTISTIC physics-based electrode manufacturing models simulating the slurry, drying, and the resulting electrode calendering, to raise a synthetic dataset that contains representative parameters of these manufacturing steps with various resulting electrode properties. Indeed, the application of low-discrepancy sequences enabled us to generate a shortened but sufficient batch of manufacturing parameter values to successfully implement deterministic learning models embedded within a multi-objective optimization loop. The deterministic learning allowed combining manufacturing parameters for calculating the electrode properties with the advantage of being computationally cheaper (a few seconds for the predictions) than the physics-based modeling chain. This characteristic made possible a fast minimization of the objective function using a Bayesian Optimization algorithm. Furthermore, we showed that the tortuosity factor, the electronic conductivity, the active surface area, and the density are bound to each other simultaneously, with the highest electrode performance expected under balanced properties.

Last but not least, we have manufactured the electrode predicted by our framework (considered as the optimal one from a modeling point of view), in order to experimentally validate the physical relevance of this prediction. As a perspective, we aim to extend our study to other manufacturing steps, such as the electrolyte infiltration, the formation, and the electrochemical performance. Also, we aim to include additional relevant manufacturing parameters (e.g., particle size, calendering speed), enlarging the interest in battery manufacturing optimization and guiding experimental protocols in our battery prototyping line for the investigation of high-performance LIB electrodes. The overall proposed approach in this article, while being demonstrated for LIBs, can be transferred to manufacture other battery technologies and the manufacturing of composite materials in general [55,80]. In addition, we believe that our approach can be adapted to optimize LIB performance and lifetime by generating synthetic data from physics-based performance models accounting for multiple aging mechanisms (e.g., SEI formation, lithium plating) and manufacturing-related parameters (e.g., particle size distribution, drying rate). This can lead to new ways of analyzing LIB degradation mechanisms to increase their performances in terms of energy, power density, and durability. Finally, we believe that our approach also paves the way towards the design of hardware/software infrastructures allowing to gather in a smart way experimental data for improving the training of Machine Learning models. This key point will enable to perform autonomous optimization in battery manufacturing processes. Such infrastructures could be built on top of on-the-fly experimental data acquisition (e.g., electrode thickness), to evaluate the process parameters to adopt being sent as instructions to actuators tuning the machines within the production or prototyping line manufacturing the electrodes. Such a futuristic vision has the potential to transform the way we optimize battery manufacturing processes, accelerating the energy transition of our societies.

Materials availability

This study did not generate new unique materials.

CRediT authorship contribution statement

Marc Duquesnoy: Conceptualization, Methodology, Investigation, Formal analysis, Software, Writing – original draft, Writing – review & editing, Resources. **Chaoyue Liu:** Investigation, Writing – review & editing, Resources. **Diana Zapata Dominguez:** Investigation, Writing –

review & editing. **Vishank Kumar:** Writing – review & editing. **Elixabete Ayerbe:** Writing – review & editing, Supervision. **Alejandro A. Franco:** Conceptualization, Methodology, Resources, Writing – review & editing, Funding acquisition, Supervision, Project administration.

Declaration of Competing Interest

The authors declare that they have no known competing interest or personal relationships that could have appeared to influence the work reported in this article.

Data availability

The used physics-based models are available via <https://www.erc-artistic.eu/computational-portal>. The data used in this work will be

made available via this project website. Other scripts are available upon reasonable request.

Acknowledgment

A.A.F., C.L. and D.Z.D. acknowledge the European Union's Horizon 2020 research and innovation program for the funding support through the European Research Council (grant agreement 772873, ARTISTIC project). M.D., E.A. and A.A.F. acknowledge the ALISTORE European Research Institute for funding support. A.A.F. acknowledges the Institut Universitaire de France for the support. We acknowledge Dr. Franco Zanotto, Dr. Mehdi Chouchane, and Dr. Teo Lombardo, all from Prof. A. A. Franco's team for assistance provided for the calculations of conductivities, tortuosity factors, densities and active surfaces.

Supplementary materials

Supplementary material associated with this article can be found, in the online version, at doi:[10.1016/j.ensm.2022.12.040](https://doi.org/10.1016/j.ensm.2022.12.040).

Appendix

A. Experimental

A.1. Electrode processing

In order to prepare the electrode, we used $\text{LiNi}_{1/3}\text{Mn}_{1/3}\text{Co}_{1/3}\text{O}_2$ (NMC111), active material supplied by Umicore. We employed C-NERGYTM super C45 carbon black (CB) supplied by IMERYS. SolefTM Polyvinylidene fluoride (PVDF) was used as a binder and purchased from Solvay, and N-methyl pyrrolidone (NMP) was used as a solvent from BASF. The slurry components (90% NMC111, 6% CB, and 4% PVDF) were premixed with a soft blender. Afterward, NMP was added until reaching a desired solid content (SC) of 57 %, a ratio between the solid components and the solvent. The mixture was performed in a Dispermat CV3-PLUS high-shear mixer for 2 hours in a water-bath cooled recipient at 25 °C. The slurry was coated over a 22 µm thick Aluminum current collector using a comma-coater prototype-grade machine (PDL250, People & Technology, Korea), fixing the gap at 90 µm and the coating speed at 0.3 m/min. The electrodes were dried in a built-in two-part oven at 80 and 95 °C. The electrodes were calendered with a prototype-grade lap press calender (BPN250, People & Technology, Korea). The latter consists of a two-roll compactor of 25 cm in diameter. The gap between the rolls was set at 37 µm to reach 30 % of compression. The calendering was performed at constant line speed (0.54 m/min) and 60 °C. The properties of the electrode are presented in Table 4. EIS tests for calculating the tortuosity were performed in 2035 coin cells assembled in a dry room ($\text{H}_2\text{O} \leq 15$ ppm). The coin cells (both on the positive and negative side) were assembled using Celgard 2500 as separator (thickness = 25 µm, porosity = 55%, mass = 2.25 mg), NMC cathodes (diameter = 13 mm, mass = 16.4 +/- 0.2 mg), positive and negative casing (mass = 0.8715 and 0.8606 g, respectively), two current collectors (thickness = 0.5 and 1.0 mm, mass = 0.758 and 1.541 g, respectively), and a spring (mass = 0.1780 g). The electrolyte was a 10 mM TBAClO_4 solution, prepared in a 1:1 wt mixture of ethylene carbonate:dimethyl carbonate (volume = 100 µL, mass = 0.148 g). The total battery mass was 4.33 +/- 0.01 g. The EIS tests were performed with an MTZ-35 impedance analyzer (BioLogic, Seyssinet-Pariset, France) in $10^1 - 10^7$ Hz with a potential perturbation of 5 mV. All measurements were carried out at 25 +/- 1 °C. The effective electronic conductivity was not characterized due to inapt experimental conditions. The measurements of ionic conductivity require specific experimental procedures for obtaining results in the liquid phase, which we were unable to attain, for instance, unsticking the current collector from the electrode and finding a suitable liquid phase.

B. Computational

B.1. Deterministic learning details

The SISSO algorithm fitted each electrode property separately. For each of them, the dimension of the descriptors was fixed to 3, and we applied the usual algebraic operations to build the descriptors (+, -, *, 2 , 3 , $^{-1}$, $\log()$, $\exp()$, $\sqrt{}$, $\sqrt[3]{}$). To evaluate the best set of descriptors when minimizing the error between the real electrode properties and the predicted one when training the model, the l_0 -norm regularization was used.

B.2. Validation metrics

The root mean square error in percentage (RMSE%) is defined by

$$\text{RMSE\%} = \sqrt{\frac{1}{4} \sum_{i=1}^n \frac{(y_i - \tilde{y}_i)^2}{\tilde{y}_i^2}} \quad (4)$$

The R^2_{score} is defined by

$$R^2_{\text{score}} = 1 - \frac{\sum_{i=1}^n (y_i - \tilde{y}_i)^2}{\sum_{i=1}^n (y_i - \bar{y})^2} \quad (5)$$

where y_i, \tilde{y}_i , and \bar{y} are the predicted values by the deterministic learning, the real value from the synthetic dataset, and the average of the real values respectively.

B.3. Bayesian optimization

Bayesian Optimization (BO) aims to minimize (C_f) by approximating it with a Gaussian Process (GP) regression model, that takes into account a batch of input manufacturing conditions $D = x_1, x_2, x_3, \dots, x_k$ and the associated objective values $C_f(x_1), C_f(x_2), C_f(x_3), \dots, C_f(x_k)$. Given the prior knowledge over $\bar{C}_f = [C_f(x_1), C_f(x_2), C_f(x_3), \dots, C_f(x_k)]$, the BO assigns a multivariate Gaussian distribution

$$\bar{C}_f \sim GP(\mu_0(x_{1:k}), \Sigma_0(x_{1:k})) \quad (6)$$

where μ_0 and Σ_0 are the expectation vector and covariance matrix respectively.

Then, the GP model has to infer the posterior distribution $(C_f | D)$ which is assumed to follow a Gaussian distribution as

$$(C_f | D) \sim GP(\mu_*(x_{1:k}), \Sigma_*(x_{1:k})) \quad (7)$$

the hyperparameters of the GP regression model are

$$\begin{Bmatrix} \mu_*(x) \\ \sigma_*(x) \end{Bmatrix} = \begin{Bmatrix} \Sigma_0(x, x_{1:k}) \Sigma_0(x_{1:k}, x_{1:k})^{-1} (\bar{C}_f - \mu_0(x_{1:k})) + \mu_0(x) \\ \Sigma_0(x, x) - \Sigma_0(x, x_{1:k}) \Sigma_0(x_{1:k}, x_{1:k})^{-1} \Sigma_0(x_{1:k}, x) \end{Bmatrix} \quad (8)$$

Once this is done, the BO decides the next condition to test to update the GP regression model at the end, and repeats the process. This choice lies on the acquisition function balancing between the exploitation and the exploration. Most of the time, the choice of the acquisition falls on either the lower confidence bound (LCB), the negative expected improvement (EI), or the negative probability of improvement (PI). In our case study, we have decided to increment a combination of those three functions (called Gaussian Process Hedge), by including a probabilistic choice from the past performances of the acquisition functions.

B.4. Acquisition function

In each step of the BO, the next condition to test x^* depends on the one proposed by the LCB, EI and PI functions. Indeed, the probabilistic choice includes the following steps after initializing a certain gain $(g_i)_{(i \leq 3)}$ to 0: (i) propose three candidates \tilde{x}_i from the different acquisition functions, (ii) choose the next conditions x^* by calculating $\text{softmax}(\eta, g_i)$ ($\eta \geq 0$), (iii) update the GP model with (x^*, y^*) ($y^* \sim C_f(x^*)$) in order to increase the size of the dataset to calculate the prior knowledge, (iv) update the gains by $g_i = g_i - \mu_0(\tilde{x}_i)$.

References

- [1] Matthew Li, Jun Lu, Zhongwei Chen, Khalil Amine, 30 years of lithium-ion batteries, *Adv. Mater.* 30 (33) (2018), 1800561.
- [2] Yangtao Liu, Ruihan Zhang, Jun Wang, Yan Wang, Current and future lithium-ion battery manufacturing, *ISCIENCE* 24 (4) (2021), 102332.
- [3] III David L Wood, Jianlin Li, Claus Daniel, Prospects for reducing the processing cost of lithium ion batteries, *J. Power Sources* 275 (2015) 234–242.
- [4] Philip Cooke, Gigafactory logistics in space and time: Tesla's fourth gigafactory and its rivals, *Sustainability* 12 (5) (2020) 2044.
- [5] Jessie E Harlow, Xiaowei Ma, Jing Li, Eric Logan, Yulong Liu, Ning Zhang, Lin Ma, Stephen L Glazier, Marc ME Cormier, Matthew Genovese, et al., A wide range of testing results on an excellent lithium-ion cell chemistry to be used as benchmarks for new battery technologies, *J. Electrochem. Soc.* 166 (13) (2019) A3031.
- [6] Yu-Ming Zhao, Feng-Shu Yue, Shi-Cheng Li, Yu Zhang, Zhong-Rong Tian, Quan Xu, Sen Xin, Yu-Guo Guo, Advances of polymer binders for silicon-based anodes in high energy density lithium-ion batteries, *InfoMat* 3 (5) (2021) 460–501.
- [7] Chris Meyer, Malte Kosfeld, Wolfgang Haselrieder, Arno Kwade, Process modeling of the electrode calendering of lithium-ion batteries regarding variation of cathode active materials and mass loadings, *J. Energy Storage* 18 (2018) 371–379.
- [8] Linda Gaines, Qiang Dai, John T Vaughey, Samuel Gillard, Direct recycling R&D at the recell center, *Recycling* 6 (2) (2021) 31.
- [9] Jianlin Li, James Fleetwood, W Blake Hawley, William Kays, From materials to cell: state-of-the-art and prospective technologies for lithium-ion battery electrode processing, *Chem. Rev.* 122 (1) (2021) 903–956.
- [10] Olivier Rynne, Matthieu Dubarry, Corentin Molson, David Lepage, Arnaud Prébé, David Aymé-Perron, Dominic Rochefort, Mickael Dollé, Designs of experiments for beginners: A quick start guide for application to electrode formulation, *Batteries* 5 (4) (2019) 72.
- [11] Thomas Kornas, Dominik Wittmann, Rüdiger Daub, Oliver Meyer, Claus Weihs, Sebastian Thiede, Christoph Herrmann, Multi-criteria optimization in the production of lithium-ion batteries, *Procedia Manuf.* 43 (2020) 720–727.
- [12] Shaosen Su, Wei Li, Yongsheng Li, Akhil Garg, Liang Gao, Quan Zhou, Multi-objective design optimization of battery thermal management system for electric vehicles, *Appl. Therm. Eng.* 196 (2021), 117235.
- [13] Teo Lombardo, Jean-Baptiste Hoock, Emiliano N Primo, Alain C Ngandjong, Marc Duquesnoy, Alejandro A Franco, Accelerated optimization methods for force-field parametrization in battery electrode manufacturing modeling, *Batteries Supercaps* 3 (8) (2020) 721–730.
- [14] Yuqian Lu, Chao Liu, I Kevin, Kai Wang, Huiyue Huang, Xun Xu, Digital twin-driven smart manufacturing: Connotation, reference model, applications and research issues, *Rob. Comput. Integr. Manuf.* 61 (2020), 101837.
- [15] Elixabete Ayerbe, Maitane Berecibar, Simon Clark, Alejandro A Franco, Janna Ruhland, Digitalization of battery manufacturing: current status, challenges, and opportunities, *Adv. Energy Mater.* 12 (17) (2022), 2102696.
- [16] Abbos Shodiev, Franco M Zanotto, Jia Yu, Mehdi Chouchane, Jianlin Li, Alejandro A Franco, Designing electrode architectures to facilitate electrolyte infiltration for lithium-ion batteries, *Energy Storage Mater.* 49 (2022) 268–277.
- [17] ARTISTIC Project website. <https://www.erc-artistic.eu>. Accessed on September 2022.
- [18] Alejandro A Franco, Alexis Rucci, Daniel Brandell, Christine Frayret, Miran Gabersek, Piotr Jankowski, Patrik Johansson, Boosting rechargeable batteries R&D by multiscale modeling: myth or reality? *Chem. Rev.* 119 (7) (2019) 4569–4627.
- [19] Teo Lombardo, Alain C Ngandjong, Amal Belhcen, Alejandro A Franco, Carbon-binder migration: a three-dimensional drying model for lithium-ion battery electrodes, *Energy Storage Mater.* 43 (2021) 337–347.
- [20] Alain C Ngandjong, Teo Lombardo, Emiliano N Primo, Mehdi Chouchane, Abbos Shodiev, Oier Arcelus, Alejandro A Franco, Investigating electrode calendering and its impact on electrochemical performance by means of a new discrete element method model: Towards a digital twin of li-ion battery manufacturing, *J. Power Sources* 485 (2021), 229320.
- [21] Abbos Shodiev, Emiliano Primo, Oier Arcelus, Mehdi Chouchane, Markus Osenberg, André Hilger, Ingo Manke, Jianlin Li, Alejandro A Franco, Insight on electrolyte infiltration of lithium ion battery electrodes by means of a new three-dimensional-resolved lattice boltzmann model, *Energy Storage Mater.* 38 (2021) 80–92.
- [22] Mehdi Chouchane, Alejandro A Franco, Deconvoluting the impacts of the active material skeleton and the inactive phase morphology on the performance of lithium ion battery electrodes, *Energy Storage Mater.* 47 (2022) 649–655.
- [23] Mehdi Chouchane, Alexis Rucci, Teo Lombardo, Alain C Ngandjong, Alejandro A Franco, Lithium ion battery electrodes predicted from manufacturing simulations: Assessing the impact of the carbon-binder spatial location on the electrochemical performance, *J. Power Sources* 444 (2019), 227285.
- [24] Chaoyue Liu, Teo Lombardo, Jiahui Xu, Alain C. Ngandjong, and Alejandro A. Franco. An experimentally-validated 3D electrochemical model revealing electrode manufacturing parameters' effects on battery performance, *Energy Storage Materials* 54 (2023) 156–163.
- [25] Chaoyue Liu, Oier Arcelus, Teo Lombardo, Hassan Oularbi, Alejandro A Franco, Towards a 3d-resolved model of Si/graphite composite electrodes from manufacturing simulations, *J. Power Sources* 512 (2021), 230486.
- [26] Teo Lombardo, Fernando Caro, Alain C Ngandjong, Jean-Baptiste Hoock, Marc Duquesnoy, Jean Charles Delapine, Adrien Ponchelet, Sylvain Doison, Alejandro A Franco, The artistic online calculator: exploring the impact of lithium-ion battery electrode manufacturing parameters interactively through your browser, *Batteries Supercaps* 5 (3) (2022), e202100324.

- [27] Ulrike Krewer, Fridolin Röder, Eranda Harinath, Richard D Braatz, Benjamin Bedürftig, Rolf Findeisen, Dynamic models of li-ion batteries for diagnosis and operation: a review and perspective, *J. Electrochim. Soc.* 165 (16) (2018) A3656.
- [28] Stavros X Drakopoulos, Azarmidokht Gholampour-Shirazi, Paul MacDonald, Robert C Parini, Carl D Reynolds, David L Burnett, Ben Pye, Kieran B O'Regan, Guanmei Wang, Thomas M Whitehead, et al., Formulation and manufacturing optimization of lithium-ion graphite-based electrodes via machine learning, *Cell Rep. Phys. Sci.* 2 (12) (2021), 100683.
- [29] Gao-Long Zhu, Chen-Zi Zhao, Jia-Qi Huang, Chuanxin He, Jian Zhang, Shaohai Chen, Lei Xu, Hong Yuan, Qiang Zhang, Fast charging lithium batteries: recent progress and future prospects, *Small* 15 (15) (2019), 1805389.
- [30] Marc Duquesnoy, Teo Lombardo, Mehdi Chouchane, Emiliano N Primo, Alejandro A Franco, Data-driven assessment of electrode calendering process by combining experimental results, *in silico* mesostructures generation and machine learning, *J. Power Sources* 480 (2020), 229103.
- [31] Ricardo Pinto Cunha, Teo Lombardo, Emiliano N Primo, Alejandro A Franco, Artificial intelligence investigation of nmc cathode manufacturing parameters interdependencies, *Batteries Supercaps* 3 (1) (2020) 60–67.
- [32] Yu-Ting Chen, Marc Duquesnoy, Darren HS Tan, Jean-Marie Doux, Hedi Yang, Grayson Deysher, Phillip Ridley, Alejandro A Franco, Ying Shirley Meng, Zheng Chen, Fabrication of high-quality thin solid-state electrolyte films assisted by machine learning, *ACS Energy Lett.* 6 (4) (2021) 1639–1648.
- [33] Mona Faraji Niri, Kailong Liu, Geanina Apachitei, Luis AA Román-Ramírez, Michael Lain, Dhammadka Widanage, James Marco, Quantifying key factors for optimised manufacturing of li-ion battery anode and cathode via artificial intelligence, *Energy AI* 7 (2022), 100129.
- [34] Mona Faraji Niri, Kailong Liu, Geanina Apachitei, Luis Roman Ramirez, Michael Lain, Dhammadka Widanage, James Marco, Machine learning for optimised and clean li-ion battery manufacturing: Revealing the dependency between electrode and cell characteristics, *J. Clean. Prod.* 324 (2021), 129272.
- [35] Teo Lombardo, Marc Duquesnoy, Hassna El-Bouysidy, Fabian Årén, Alfonso Gallo-Bueno, Peter Björn Jørgensen, Arghya Bhownik, Arnaud Demortière, Elixabete Ayerbe, Francisco Alcaide, Marine Reynaud, Javier Carrasco, Alexis Grimaud, Chao Zhang, Tejs Vegge, Patrik Johansson, Alejandro A. Franco, Artificial intelligence applied to battery research: hype or reality?, *Chem. Rev.* 122 (12) (2022) 10899.
- [36] Zheming Tong, Jiazhi Miao, Shuguang Tong, Yingying Lu, Early prediction of remaining useful life for lithium-ion batteries based on a hybrid machine learning method, *J. Cleaner Prod.* 317 (2021), 128265.
- [37] Artem Turetskyy, Jacob Wessel, Christoph Herrmann, Sebastian Thiede, Battery production design using multi-output machine learning models, *Energy Storage Mater.* 38 (2021) 93–112.
- [38] Jie Bao, Vijayakumar Murugesan, Carl Justin Kamp, Yuyan Shao, Litao Yan, Wei Wang, Machine learning coupled multi-scale modeling for redox flow batteries, *Adv. Theory Simul.* 3 (2) (2020), 1900167.
- [39] Anthony Barré, Benjamin Deguilhem, Sébastien Grolleau, Mathias Gérard, Frédéric Suard, Delphine Riu, A review on lithium-ion battery ageing mechanisms and estimations for automotive applications, *J. Power Sources* 241 (2013) 680–689.
- [40] Michael A Gennert, Alan L Yuille, Determining the optimal weights in multiple objective function optimization, in: *ICCV*, 1988, pp. 87–89.
- [41] Francesco Archetti, Antonio Candelieri, *Bayesian Optimization and Data Science*, Springer, 2019.
- [42] Tinkle Chugh, Yaochu Jin, Kaisa Miettinen, Jussi Hakkanen, Karthik Sindhya, A surrogate-assisted reference vector guided evolutionary algorithm for computationally expensive many-objective optimization, *IEEE Trans. Evol. Comput.* 22 (1) (2016) 129–142.
- [43] Bobak Shahriari, Kevin Swersky, Ziyu Wang, Ryan P Adams, Nando De Freitas, Taking the human out of the loop: a review of Bayesian optimization, *Proc. IEEE* 104 (1) (2015) 148–175.
- [44] Romy Lorenz, Adam Hampshire, Robert Leech, Neuroadaptive bayesian optimization and hypothesis testing, *Trends Cogn. Sci.* 21 (3) (2017) 155–167.
- [45] Eric Brochu, Vlad M Cora, and Nando De Freitas, A tutorial on bayesian optimization of expensive cost functions, with application to active user modeling and hierarchical reinforcement learning, *arXiv preprint arXiv:1012.2599*, 2010.
- [46] Syusuke Sano, Tadashi Kadokawa, Koji Tsuda, Susumu Kimura, Application of bayesian optimization for pharmaceutical product development, *J. Pharmaceut. Innov.* 15 (3) (2020) 333–343.
- [47] Ke Wang, Alexander W Dowling, Bayesian optimization for chemical products and functional materials, *Curr. Opin. Chem. Eng.* 36 (2022), 100728.
- [48] Benben Jiang, Marc D Berliner, Kun Lai, Patrick A Asinger, Hongbo Zhao, Patrick K Herring, Martin Z Bazant, Richard D Braatz, Fast charging design for lithium-ion batteries via bayesian optimization, *Appl. Energy* 307 (2022), 118244.
- [49] Ashwin Gaonkar, Homero Valladares, Andres Tovar, Likun Zhu, Hazim El-Mounayri, Multi-objective bayesian optimization of lithium-ion battery cells for electric vehicle operational scenarios, *Electron. Mater.* 3 (2) (2022) 201–217.
- [50] A Mamun, I Narayanan, D Wang, A Sivasubramaniam, HK Fathy, Multi-objective optimization of demand response in a datacenter with lithium-ion battery storage, *J. Energy Storage* 7 (2016) 258–269.
- [51] Siddhartha Mishra, T Konstantin Rusch, Enhancing accuracy of deep learning algorithms by training with low-discrepancy sequences, *SIAM J. Numer. Anal.* 59 (3) (2021) 1811–1834.
- [52] Carolina Furtado, LF Pereira, Rodrigo Paiva Tavares, M Salgado, F Otero, Giuseppe Catalaniotti, Albertino Arteiro, Miguel A Bessa, Pedro P Camanho, A methodology to generate design allowables of composite laminates using machine learning, *Int. J. Solids Struct.* 233 (2021), 111095.
- [53] De Rainville et al. Design d'expérimentation interactif: aide à la compréhension de systèmes complexes. 2010.
- [54] Cristiano Cervellera, Marco Muselli, Deterministic design for neural network learning: An approach based on discrepancy, *IEEE Trans. Neural Networks* 15 (3) (2004) 533–544.
- [55] Teo Lombardo, Fanny Lambert, Roberto Russo, Franco M Zanotto, Christine Frayret, Gwenaelle Toussaint, Philippe Stevens, Matthieu Becuwe, Alejandro A Franco, Experimentally validated three-dimensional modeling of organic-based sodium-ion battery electrode manufacturing, *Batteries & Supercaps* (2022), e202200116.
- [56] RS2E prototyping unit. <https://www.energie-rs2e.com/fr/unite-de-prototypage>. Accessed on September 2022.
- [57] Benjamin FrantzDale, Steven J Plimpton, Mark S Shephard, Software components for parallel multiscale simulation: an example with lammps, *Eng. Comput.* 26 (2) (2010) 205–211.
- [58] Math2Market. Geodict startpage. <https://www.math2market.com/>. Accessed on September 2022.
- [59] Samuel J Cooper, Antonio Bertei, Paul R Shearing, JA Kilner, Nigel P Brandon, Taufactor: an open-source application for calculating tortuosity factors from tomographic data, *SoftwareX* 5 (2016) 203–210.
- [60] Moe Elbadawi, Simon Gaisford, Abdul W Basit, Advanced machine-learning techniques in drug discovery, *Drug Discov. Today* 26 (3) (2021) 769–777.
- [61] Runhai Ouyang, Stefano Curtarolo, Emre Ahmetcik, Matthias Scheffler, Luca M Ghiringhelli, Sisso: a compressed-sensing method for identifying the best low-dimensional descriptor in an immensity of offered candidates, *Phys. Rev. Mater.* 2 (8) (2018), 083802.
- [62] Runhai Ouyang, Emre Ahmetcik, Christian Carbogno, Matthias Scheffler, Luca M Ghiringhelli, Simultaneous learning of several materials properties from incomplete databases with multi-task sisso, *J. Phys.: Mater.* 2 (2) (2019), 024002.
- [63] Isabelle Guyon, André Elisseeff, An introduction to variable and feature selection, *J. Mach. Learn. Res.* 3 (Mar) (2003) 1157–1182.
- [64] Philip Breen, Algorithms for sparse approximation, in: *School of Mathematics*, 4, University of Edinburgh, 2009, Year.
- [65] Jianqing Fan, Jinchu Lv, Sure independence screening for ultrahigh dimensional feature space, *J. R. Stat. Soc.: Ser. B (Stat. Methodol.)* 70 (5) (2008) 849–911.
- [66] Gustavo Malkomes, Charles Schaff, Roman Garnett, Bayesian optimization for automated model selection, *Adv. Neural Inf. Process. Syst.* 29 (2016).
- [67] Hu Zhang, Jianyong Sun, Tonglin Liu, Ke Zhang, Qingfu Zhang, Balancing exploration and exploitation in multiobjective evolutionary optimization, *Inf. Sci.* 497 (2019) 129–148.
- [68] Michael Adam Gelbart. Constrained Bayesian optimization and applications. PhD thesis, 2015.
- [69] Carlos A Coello Coello, Gary B Lamont, David A Van Veldhuizen, et al., *Evolutionary Algorithms for Solving Multi-Objective Problems*, 5, Springer, 2007.
- [70] Zuzana Reitermanova, et al., Data splitting, in: *In WDS*, 10, Matfyzpress Prague, 2010, pp. 31–36.
- [71] Bo Jiang, Xuegong Zhang, Tianxi Cai, Estimating the confidence interval for prediction errors of support vector machine classifiers, *J. Mach. Learn. Res.* 9 (2008) 521–540.
- [72] Geoff Cumming, Robert Calin-Jageman, *Introduction to the new statistics: Estimation, open science, and beyond*, Routledge (2016).
- [73] Partial dependence plot. <https://christophm.github.io/interpretable-ml-book/pdp.html>. Accessed on September 2022.
- [74] Arnulf Latz, Jochen Zausch, Thermodynamic derivation of a butler-volmer model for intercalation in li-ion batteries, *Electrochim. Acta* 110 (2013) 358–362.
- [75] Severin Vierrath, Lukas Zielke, Riko Moroni, Andrew Mondon, Dean R Wheeler, Roland Zengerle, Simon Thiele, Morphology of nanoporous carbon-binder domains in li-ion batteries – a fib-sem study, *Electrochim. Commun.* 60 (2015) 176–179.
- [76] Bradley L Trembacki, Aashutosh N Mistry, David R Noble, Mark E Ferraro, Partha P Mukherjee, Scott A Roberts, Mesoscale analysis of conductive binder domain morphology in lithium-ion battery electrodes, *J. Electrochim. Soc.* 165 (13) (2018) E725.
- [77] Johannes Landesfeind, Johannes Hattendorff, Andreas Ehrl, Wolfgang A Wall, Hubert A Gasteiger, Tortuosity determination of battery electrodes and separators by impedance spectroscopy, *J. Electrochim. Soc.* 163 (7) (2016) A1373.
- [78] Marc Duquesnoy, Teo Lombardo, Fernando Caro, Florent Haudiquez, Alain C Ngandjoung, Jiahui Xu, Hassan Oularbi, and Alejandro A Franco. Functional data-driven framework for fast forecasting of electrode slurry rheology simulated by molecular dynamics. *npj Comput Mater* 8, 161 (2022).
- [79] Jiahui Xu, Alain C Ngandjoung, Chaoyue Liu, Franco M Zanotto, Oier Arcelus, Arnaud Demortiere, and Alejandro A Franco. Lithium ion battery electrode manufacturing model accounting for 3d realistic shapes of active material particles. *J. Power Sources*, 554 (2023) 232294.
- [80] Oier Arcelus, Alejandro A Franco, Perspectives on manufacturing simulations of Li-S battery cathodes, *J. Phys.: Energy* 4 (1) (2022), 011002.